

Time-resolved gamma spectroscopy of single events

Wolszczak, W.; Dorenbos, P.

DOI

[10.1016/j.nima.2017.12.080](https://doi.org/10.1016/j.nima.2017.12.080)

Publication date

2018

Document Version

Accepted author manuscript

Published in

Nuclear Instruments and Methods in Physics Research, Section A: Accelerators, Spectrometers, Detectors and Associated Equipment

Citation (APA)

Wolszczak, W., & Dorenbos, P. (2018). Time-resolved gamma spectroscopy of single events. *Nuclear Instruments and Methods in Physics Research, Section A: Accelerators, Spectrometers, Detectors and Associated Equipment*, 886, 30-35. <https://doi.org/10.1016/j.nima.2017.12.080>

Important note

To cite this publication, please use the final published version (if applicable). Please check the document version above.

Copyright

Other than for strictly personal use, it is not permitted to download, forward or distribute the text or part of it, without the consent of the author(s) and/or copyright holder(s), unless the work is under an open content license such as Creative Commons.

Takedown policy

Please contact us and provide details if you believe this document breaches copyrights. We will remove access to the work immediately and investigate your claim.

Time-resolved gamma spectroscopy

W. Wolszczak, P. Dorenbos

*Delft University of Technology, Faculty of Applied Sciences, Department of Radiation
Science and Technology (FAME-LMR), Mekelweg 15, 2629 JB Delft, Netherlands*

Abstract

In this article we present a method of characterizing scintillating materials by digitization of each individual scintillation pulse followed by digital signal processing. With this technique it is possible to measure the pulse shape and the energy of an absorbed gamma photon on an event-by-event basis. In contrast to other methods, the digital approach provides a shorter measurement time, an active noise suppression, and enables characterization of scintillation pulses simultaneously in two domains: time and energy. We applied this method to study the pulse shape change of a CsI(Tl) scintillator with energy of gamma excitation. We confirmed previously published results and revealed new details of the phenomenon.

Keywords: time-resolved gamma spectroscopy, pulse shape analysis, data acquisition, digital signal processing, gamma spectroscopy, CsI(Tl)

1. Introduction

Despite many years of studies on scintillating materials many questions are still open. While luminescence processes and high energy radiation interactions with matter are well understood, the fundamental processes of energy transport and high density quenching are still puzzling [1–6]. It is well known that a scintillation pulse shape changes with change of type of excitation (γ -rays, neutrons, α particles, high energy ions) [7–13]. This phenomenon is commonly used for particle discrimination in variety of applications [14–17]. However, the origin and the exact mechanism are still not known. In last years, a dependence of a

17 scintillation pulse shape on γ photons energy was reported for various materials
18 [18–21]. Recent theoretical developments [2, 3, 5, 6] provided an explanation of
19 these observations by modeling the charge separation inside the ionization track
20 created during a gamma energy excitation.

21 Despite successful results of the theoretical modeling, many aspects still
22 require an experimental study and verification. This raises a need for new data
23 and a new experimental approach. The aim of this study is to provide a new
24 method of characterizing scintillators in two domains simultaneously: in terms
25 of the excitation energy, and time evolution of scintillation.

26 We will demonstrate that by digitization of individual scintillation pulses and
27 digital signal processing it is possible to study the scintillation mechanism in
28 terms of pulse shape and light yield at the same time. For each scintillation pulse
29 it is possible to calculate the integral light output and corresponding deposited
30 amount of energy. The acquired pulse height spectrum can be later subdivided
31 into energy bins. An average scintillation pulse shape can be calculated for
32 each energy bin by taking an average of all acquired events within that bin.
33 However, to obtain undistorted pulse shapes additional signal processing and
34 event selections are required before taking the average.

35 With this method we verified previous experimental results on CsI(Tl) pulse
36 shape dependence on gamma energy, and we compared those results with the-
37 oretical models [6]. We have found that the pulse shape change predicted by
38 the model is in good agreement with the measured data, however we observed
39 some differences. The proposed method was used to characterize a scintillation
40 decay time of CsI(Tl) excited with pulsed X-rays and gamma rays. It was found
41 that X-ray excited pulses have a significantly different pulse shape. We will
42 conclude that the proposed method provides a new way of characterization of
43 scintillators.

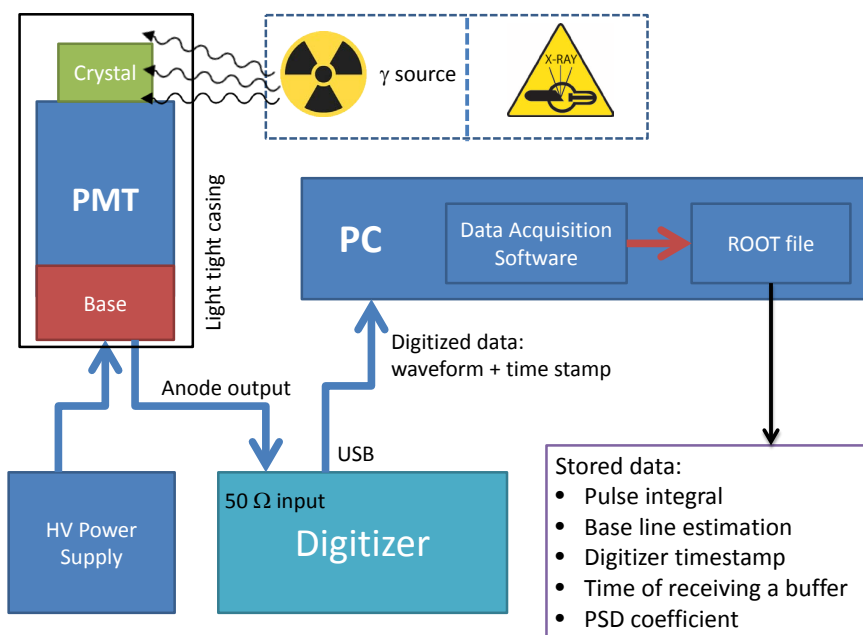


Figure 1: Schematic of the Time Resolved Gamma Spectroscopy setup. The gamma source or a pulsed X-ray tube excite the scintillation crystal. The resulting scintillation pulses are detected with a photomultiplier tube and digitized on event-by-event principle.

44 **2. Materials and methods**

45 *2.1. The setup*

46 The measuring setup is shown diagrammatically in Fig. 1. Scintillation
47 pulses from a one inch CsI(Tl) sample are converted to electrical pulses by a
48 Hamamatsu H5510 Photomultiplier Tube (PMT). The scintillation crystal is
49 optically coupled with silicon oil to the PMT's entrance window. The PMT's
50 anode signal is connected directly to the 10-bit 4 Giga Samples Per Second
51 (GSPS) DT5761 digitizer from CAEN. The digitizer has an input range of 1 Vpp,
52 input impedance $Z_{in} = 50 \Omega$, and a memory buffer depth of $7.2 \cdot 10^6$ samples.
53 No preamplifier nor other ways of analog signal shaping have been used. All
54 data acquisition and on-line processing is done with a personal computer and
55 homemade software *veroDigitizer*.

56 A ^{137}Cs source has been used for excitation. The barium X-rays (32 keV)
57 were absorbed by a lead absorber placed between the ^{137}Cs source and the
58 detector. In this way we avoided photoelectric absorption of low energy X-
59 rays, and either photoelectrons or Compton electrons from 662 keV gamma
60 interaction were detected. As an alternative to γ rays, we used a light excited
61 X-ray tube N5084 from Hamamatsu for generation of ultra short X-ray pulses
62 (<100 ps). The X-ray tube has a tungsten target and is powered with a 40 kV
63 power supply. Each X-ray pulse contains multiple X-ray photons, which enables
64 low energy excitation (~ 10 keV) but with a high light output.

65 *2.2. Data acquisition*

66 When the anode signal exceeds the digitizer's trigger voltage V_{tr} an event is
67 triggered and stored in a local buffer. Each event contains a waveform consisting
68 of 56k voltage samples ($14 \mu\text{s}$ time range). When the internal buffer is full, all
69 digitized events are transferred to the PC for data processing. In order to record
70 low energy events, the digitizer's trigger voltage V_{tr} was set as close as possible
71 to the signal's base line. However, the low V_{tr} results in pick-up of noise spikes
72 like in the exemplary pulse shown in Fig. 2. Fig. 3 shows the steps of the

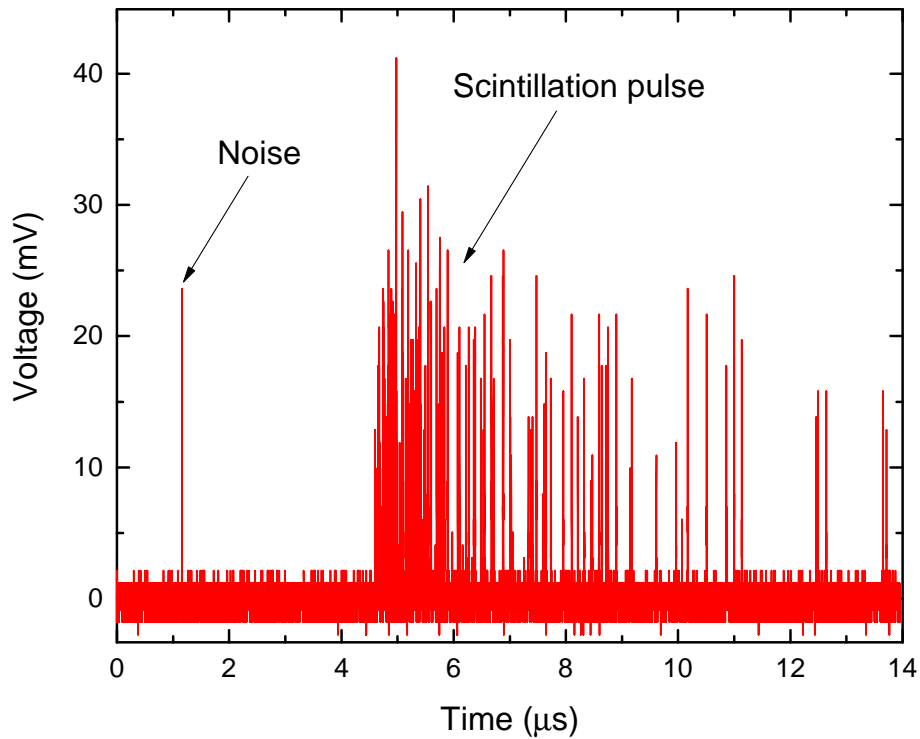


Figure 2: Event triggered by a noise spike at around $1 \mu\text{s}$ with a coincident scintillation pulse starting at around $5 \mu\text{s}$.

73 data processing which are required before the triggered events can be used for
 74 calculating average pulse shapes. Only events fulfilling multiple criteria are
 75 selected in order to remove unwanted noise events, suppress pile-up, and assure
 76 good quality of each triggered pulse. The following sections will discuss in detail
 77 each step of the data processing.

78 *2.3. Filtering and decimation*

79 The digitizer reduces a continuous-time signal from the PMT to a discrete-
 80 time digital signal (sampling). High sampling frequency of the used digitizer
 81 $f_s = 4 \text{ GHz}$ provides precise timing information, but in case of CsI(Tl) with
 82 slow decay time it results in high uncertainty of each value at a point in time
 83 of the measured signal (low signal to noise ratio), see Fig. 2 and raw signal

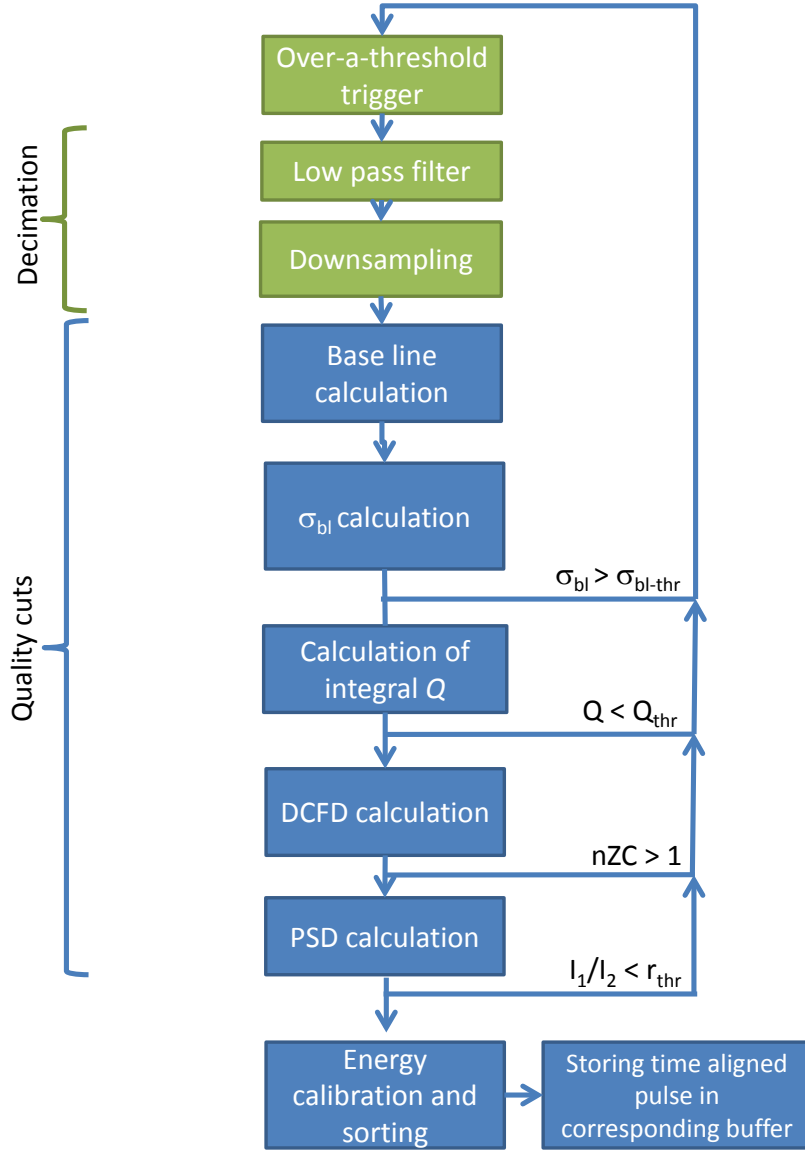


Figure 3: Diagram of data processing workflow. σ_{bl} is the standard deviation of the base line; σ_{bl-thr} is a maximum threshold for standard deviation of the base line; Q is the pulse integral; Q_{thr} is a pulse integral minimum threshold; nZC is the number of zero crossings in the Digital Constant Fraction Discriminator (DCFD) signal; I_1/I_2 is the pulse shape factor defined as the ratio of the short and long integration gates.

84 in Fig. 5. To increase the signal to noise ratio and decrease the uncertainty
 85 of a measured voltage each waveform was down-sampled (decimated) by first
 86 applying a low pass digital filter and then reducing the number of samples by a
 87 factor of $M = 256$.

88 To avoid aliasing it is needed to do a low pass filtering before downsampling
 89 [22]. The cutoff frequency of the filter has to be equal or lower than the Nyquist
 90 frequency of the down-sampled signal, which is $f_{co} = \frac{f_s/2}{M} = \frac{4000/2}{256} \approx 7.8$ MHz.
 91 Fig. 4 shows time and frequency domain responses of multiple standard digital
 92 filters designed for -3dB cutoff frequency at 7.8 MHz. Because in our measure-
 93 ments we want to preserve an undistorted time response of the signal, the filter
 94 choice is limited just to two filters: a moving average filter (length $N = 227$) or a
 95 Bessel filter. The moving average filter has the worst frequency response among
 96 considered filters. It has side lobes in the stop band, but provides the fastest
 97 rise time in response to the step input, and it is free of overshoots in the time
 98 domain. In addition, a recursive implementation of the moving average filter
 99 provides the shortest computation time compared to that of the other filters
 100 [22].

101 Each sample of the downsampled waveform $d[i]$ is calculated by taking the
 102 average value of length $M = 256$ from the filtered waveform $f[i]$ according to
 103 the formula: $d[i] = \frac{1}{M} \sum_{k=M \cdot i}^{M \cdot (i+1)} f[k]$.

104 2.4. Quality cuts

105 Selections were applied to data to remove noise events, assure proper trigger-
 106 ing time within each waveform, and to select non distorted single scintillation
 107 pulses. Fig. 3 shows the steps of the data processing. After an event decimation
 108 a baseline BL and its' standard deviation σ_{bl} are calculated. If σ_{bl} exceeds the
 109 base line standard deviation threshold σ_{bl-thr} the event is discarded and no
 110 longer processed. In this way we assure a good quality of the calculated base
 111 line. Usually σ_{bl-thr} is exceeded when random noise is present within the base
 112 line window or a scintillation pulse was triggered too late and the leading edge
 113 is before the expected triggering time.

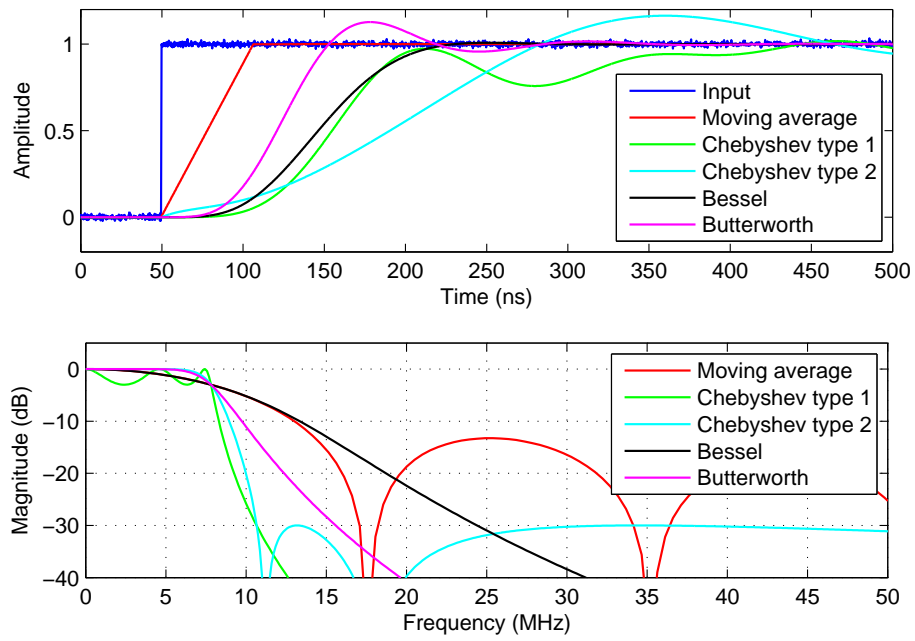


Figure 4: Comparison of five digital low pass filters in time (upper panel) and frequency domains (lower panel).

114 In the next step the integral Q of a decimated pulse is calculated using the
115 previously obtained base line: $Q = \sum_0^L (w[i] - BL)$. If the calculated Q is lower
116 than the minimum integral threshold Q_{thr} , the event is discarded and no longer
117 processed. This requirement suppresses all events which exceed the digitizer's
118 trigger threshold, but consist mostly of noise spikes, single photoelectron events,
119 afterglow pulses, or other non-scintillation pulses. This requirement is crucial
120 especially for low energy deposition events when noise is of the same order of
121 magnitude as the scintillation pulses. If not suppressed properly it can lead to
122 creation of an artificial fast component in a decay spectrum or other distortions
123 of a pulse shape.

124 Fig. 2 shows an example of a "wrong" event: a scintillation pulse appears
125 after the expected trigger point. A noise peak exceeded the trigger threshold
126 and the event was digitized and stored. The scintillation pulse which coincided
127 with the noise pulse caused that the event passed minimum energy requirement.
128 However, the leading edge of the scintillation pulse is not properly located in
129 the time window.

130 To properly measure a pulse shape it is important to suppress pile-up of
131 scintillation events within the acquisition window. In Fig. 5 the black line
132 shows a raw signal from the digitizer; the red line shows the signal after low
133 pass filtering and downsampling; the blue line shows the output of a digital
134 constant fraction discriminator (DCFD). There are two points in the figure when
135 the DCFD signal is crossing zero, which indicates that we are dealing with two
136 scintillation pulses. If more than one zero crossing $n_{ZC} > 1$ was observed within
137 the acquisition window the event was rejected from further processing. If only
138 one zero crossing was observed the event was kept for further processing, and
139 the zero crossing time was used later for aligning events in time.

140 3. Results

141 Fig. 6 shows a pulse height spectrum measured with CsI(Tl) excited with
142 662 keV γ -photons. The barium x-ray peak was successfully suppressed by the

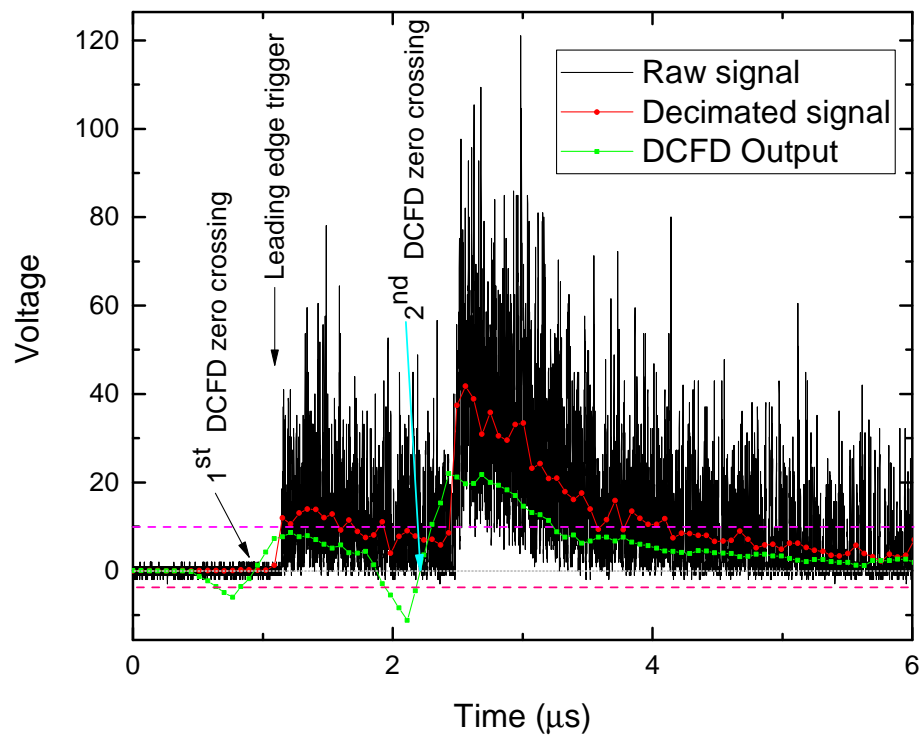


Figure 5: Exemplary pile-up event.

143 lead absorber, and only Compton scattered events are present besides the 662
 144 keV photopeak. The shown energy range was divided into 10 energy bins and
 145 an average pulse shape for each range has been calculated separately.

146 Fig. 7 shows pulse shapes of CsI(Tl) scintillation measured in multiple en-
 147 ergy subranges. The only curve that deviates significantly is for 25-97 keV
 148 energies. Another measurement was performed with the requirement that the
 149 energy deposit is lower than 184 keV to investigate better the low energy range.
 150 Fig. 8 shows the decay curves at low energy deposition. The largest difference
 151 was observed for 25-41 keV events, a very small deviation was observed in the
 152 41-89 keV range, and small but still rousignificant pulse change was observed
 153 from 89 keV to 184 keV.

154 To quantify the pulse shape change shown in Fig. 8, the decay curves were
 155 fitted with a double exponential function $f(t) = A_1 \exp(-\frac{t}{\tau_1}) + A_2 \exp(-\frac{t}{\tau_2})$,
 156 where A_1 and A_2 are the amplitudes of the fast and the slow component, and
 157 τ_1 and τ_2 are decay constants. The results of these fits are shown in Fig. 9 and
 158 Fig. 10, where intensities I_1 and I_2 were calculated as follows: $I_i = \frac{A_i * \tau_i}{A_1 * \tau_1 + A_2 * \tau_2}$.
 159 Both decay constants are decreasing with decrease of energy, but there is a 'dip'
 160 present near 60 keV. The slow component decreases from around 5.8 μ s to 4.7
 161 μ s in the studied energy range, while the fast component changes from around
 162 900 ns to 850 ns.

163 The intensity of the slow component I_2 increases with increase of energy, see
 164 Fig. 10. The intensity change deviates from being smooth at energies around
 165 50 keV, similarly to the decay components.

166 Fig. 11 shows a pulse height spectrum measured with a ^{137}Cs source together
 167 with X-ray pulses from a pulsed X-ray tube. The tube pulses are observed at
 168 deposited energy of around 1.3 MeV with FWHM of 37%. Assuming that the
 169 average energy of a single X-ray photon from the tungstate anode is around ~ 10
 170 keV, we may estimate that a single X-ray pulse leads to ~ 130 detected x-ray
 171 photons.

172 Fig. 12 compares a scintillation pulse shape of CsI(Tl) excited with high
 173 energy gamma photons (575-758 keV), low energy Compton electrons (25-96

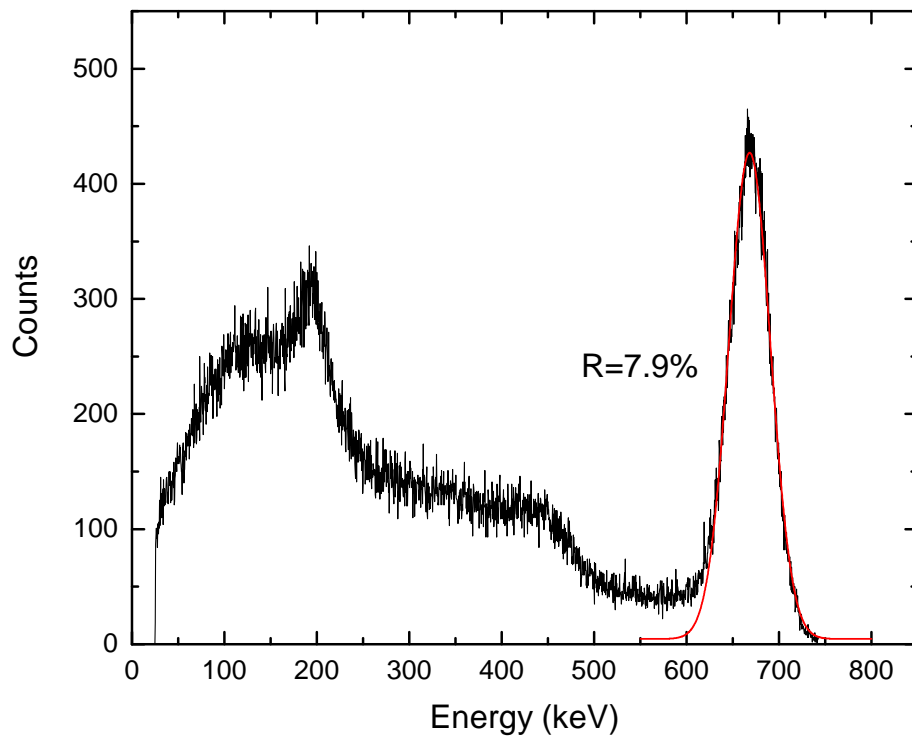


Figure 6: Pulse height spectrum of ^{137}Cs gamma source measured with CsI:TI.

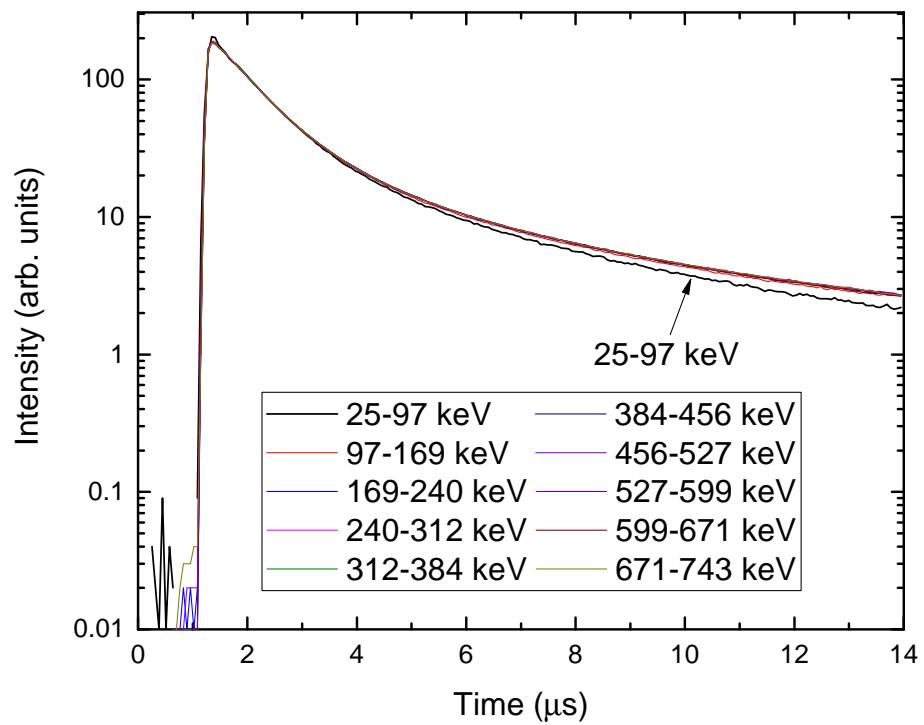


Figure 7: Energy-sorted pulse shapes of CsI(Tl) under Cs-137 excitation. Only the lowest energy range 25-97 keV displays a significantly different pulse shape.

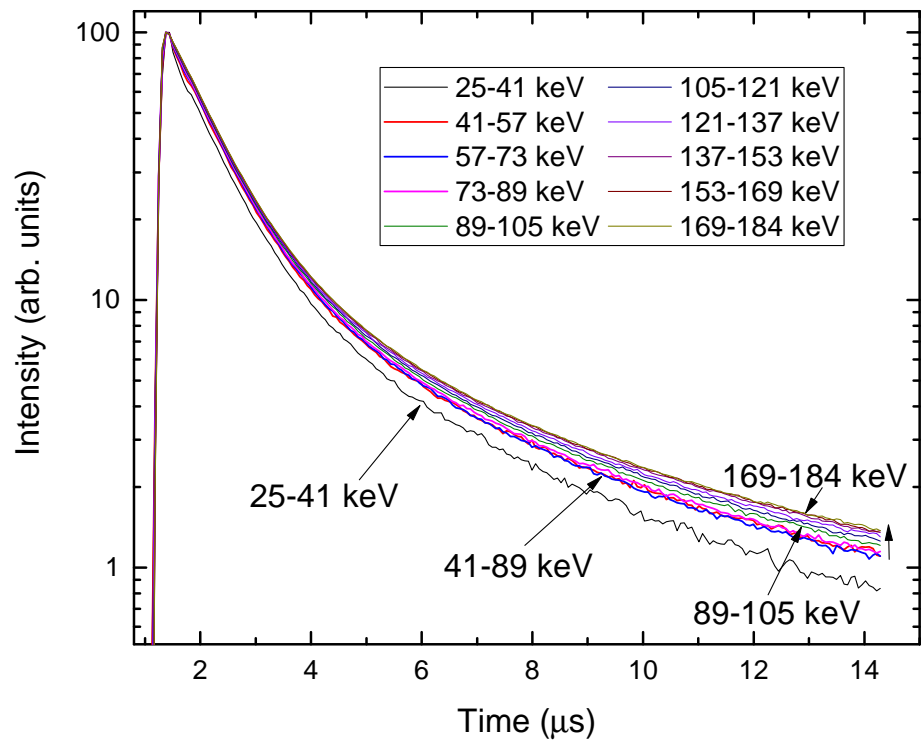


Figure 8: Energy-sorted pulse shapes of CsI(Tl) under Cs-137 excitation, events with energies lower than 228 keV.

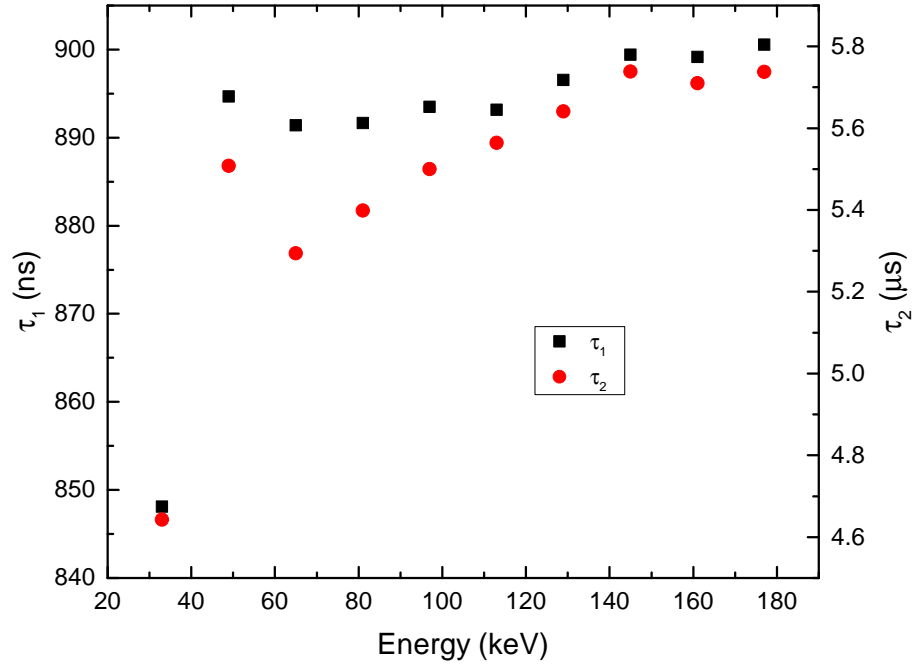


Figure 9: Decay constants of fast τ_1 and τ_2 slow luminescence decay components.

174 keV), and picosecond X-ray pulses (10 keV). Events excited by the pulsed x-
 175 ray tube exhibit the lowest intensity of the long decay component, while high
 176 energy γ photons have the highest intensity of the slow component. The pulses
 177 from Fig. 12 were fitted with a double exponential function and the results
 178 are shown in Table 1. The fast component under X-ray excitation is 6% faster
 179 compared to the 662 keV energy range. The slow decay constant decreases
 180 11% in the same energy range. The intensity of the slow component increases
 181 4.3% when the source of excitation is changed from 662 keV to X-rays. The
 182 pulse change measured with low energy deposition (25-97 keV) compared to the
 183 575-758 keV range is significantly smaller and it is less than 1% change of the
 184 fast decay component and less than 4% of the slow component. The change of
 185 intensity is around 1%.

186 The pulse shape factor was defined as a ratio of two integrals: the leading
 187 edge, and the tail part of the pulse. Length of both integrals was optimized to

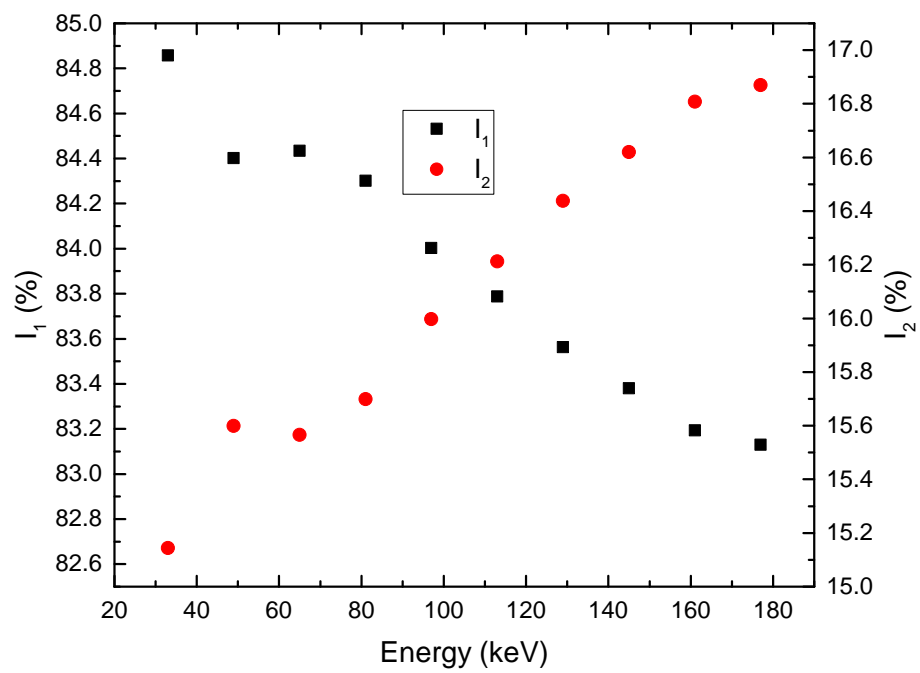


Figure 10: Intensities of fast I_1 and slow I_2 luminescence decay components.

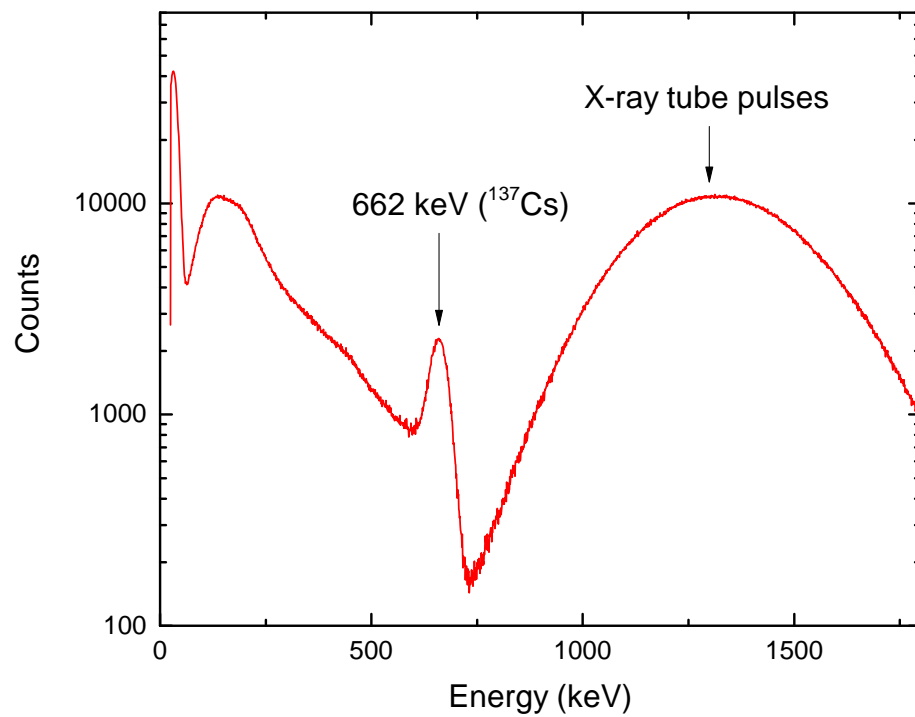


Figure 11: Pulse height spectrum measured with CsI(Tl) excited with a Cs-137 gamma source and pulsed X-ray tube.

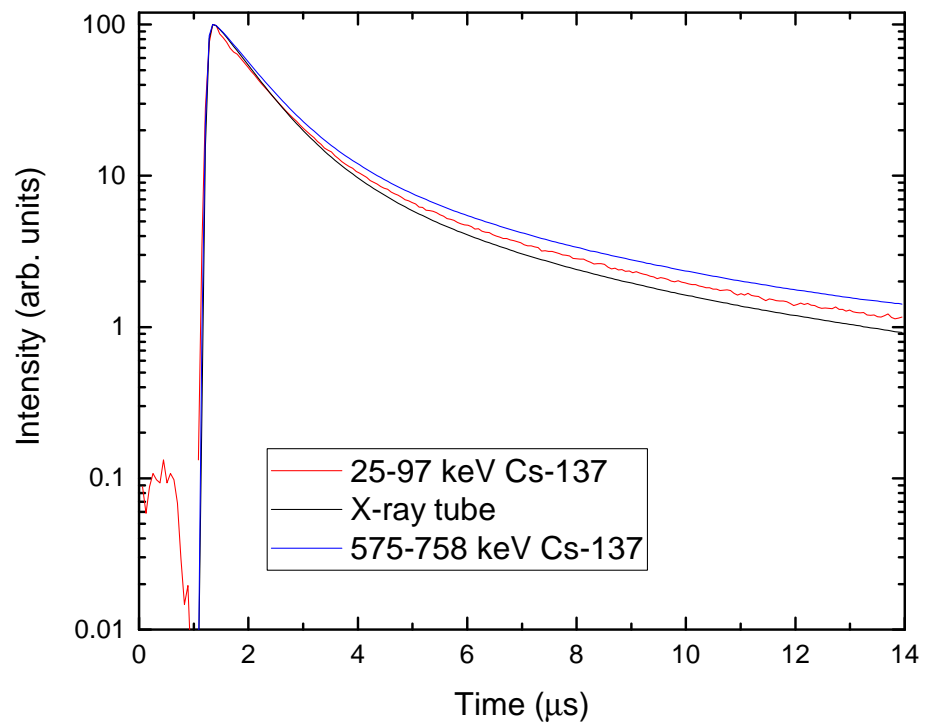


Figure 12: Comparison of CsI(Tl) scintillation pulse shape excited with Cs-137 gamma source and picosecond X-ray tube pulses.

Table 1: Decay constants and their intensities of CsI(Tl) luminescence excited with a picosecond X-ray tube, low and high energy excitation.

Excitation	τ_1 (ns)	τ_2 (μ s)	I_1 (%)	I_2 (%)
X-rays	800	4.7	87.1	12.9
25-97 keV	845	5.1	83.9	16.1
575-758 keV	850	5.3	82.8	17.2

188 get the pulse shape factor value close to one. Fig. 13 shows pulse shape factor
 189 versus energy of pulses. X-ray pulses (1000-2200 channels) have higher pulse
 190 shape factor then γ rays from Cs-137 source (662 keV at 800 channel).

191 4. Discussion

192 Lu et al. [6] provided a detailed theoretical analysis of the pulse shape
 193 dependence on gamma energy in CsI(Tl). Three possible reactions leading to
 194 luminescence were considered. Reaction 1 is the direct Tl^+ excitation by sequen-
 195 tial capture of free holes and electrons: $Tl^+ + e^- + h^+ \rightarrow (Tl^+)^* \rightarrow Tl^+ + h\nu$.
 196 Reaction 2 is the recombination of self-trapped holes with electrons trapped on
 197 Tl^0 : $Tl^0 + STH \rightarrow (Tl^+)^*$. Reaction 3 is the thermally activated release of elec-
 198 trons trapped as Tl^0 that subsequently recombine with holes trapped as Tl^{2+} :
 199 $Tl^0 + Tl^{2+} \rightarrow (Tl^+)^*$. According to Lu et al., the fast ~ 700 ns decay component
 200 can be mostly attributed to the 576 ns radiative decay of $(Tl^+)^*$ from Reaction
 201 2 and to transport limited Reaction 3, while the 3- and 17 μ s components are
 202 the rate- and transport limited phases of Reaction 3. The energy dependence
 203 of the pulse shape can be explained by the change of efficiency of the Reaction
 204 3 which is dependent on the electric field created between space-separated Tl^0
 205 and Tl^{2+} reservoirs.

206 Fig. 14 shows a comparison of the theoretical modeling results by Lu [6] and
 207 experimental data presented in this work. The model provides a good qualita-
 208 tive description of the data; the same trend and magnitude of the experimental
 209 pulse shape change is reproduced by the calculations. However, there are some

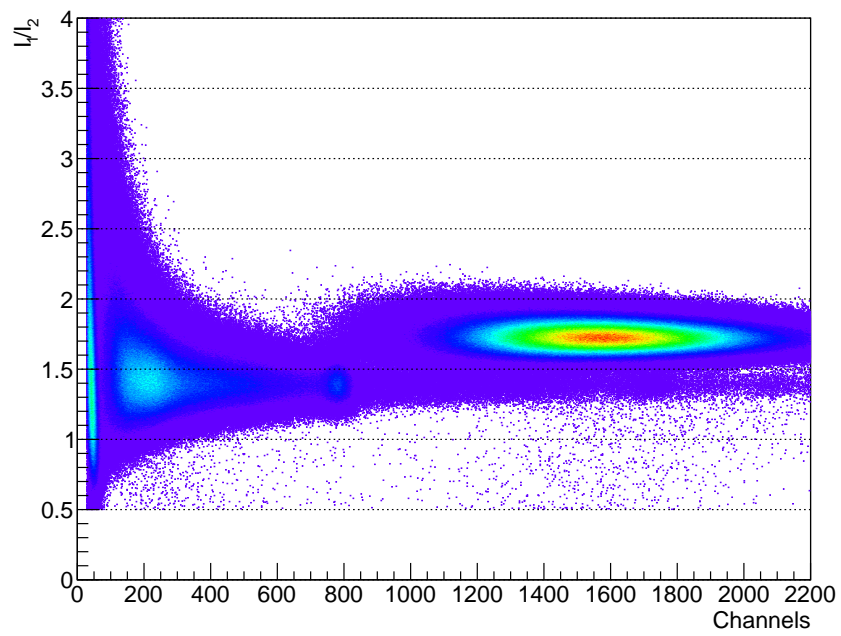


Figure 13: Pulse shape factor vs pulse integral. Scintillation pulses excited with X-ray tube exhibit a distinctively different shape.

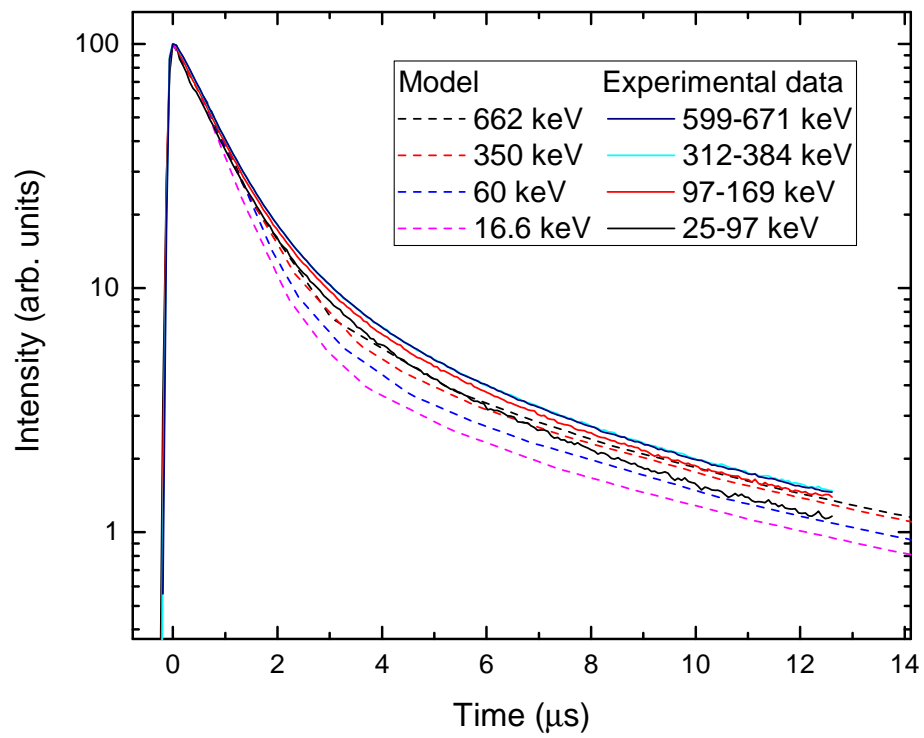


Figure 14: Comparison of the Lu model predictions [6] with the measured data.

210 discrepancies. The model does not predict correctly a change of the slow com-
211 ponent ($\sim 5 \mu\text{s}$) decay constant, and the change of the fast component (~ 800
212 ns) is predicted to be bigger than observed in experiment. Some difficulty for a
213 fair comparison is caused by the fact that the experimental data are measured
214 with limited energy resolution ranges, while theoretical predictions are provided
215 for monoenergetic gamma photons.

216 5. Conclusions

217 In this article we have presented a new method of characterizing scintillators.
218 We found a weak pulse shape dependence on gamma energy for CsI(Tl), and
219 different scintillation decay time for gamma rays and X-ray pulsed excitations.
220 The experimental results are in good agreement with theoretical predictions by
221 Lu et al. [6], but minor differences are observed and require more research.

222 6. Acknowledgments

223 This work was supported by the Dutch Technology Foundation STW, which
224 is part of the Netherlands Organization for Scientific Research (NWO), which
225 is partly funded by the Ministry of Economic Affairs. This work was partly
226 funded by Saint Gobain Crystals, France.

227 [1] P. Dorenbos, J. de Haas, and C. van Eijk, “Non-proportionality in the
228 scintillation response and the energy resolution obtainable with scintillation
229 crystals,” *IEEE Transactions on Nuclear Science*, vol. 42, pp. 2190–2202,
230 Dec 1995.

231 [2] R. T. Williams, J. Q. Grim, Q. Li, K. B. Ucer, G. A. Bizarri, S. Kerisit,
232 F. Gao, P. Bhattacharya, E. Tupitsyn, E. Rowe, V. M. Buliga, and
233 A. Burger, “Experimental and computational results on exciton/free-
234 carrier ratio, hot/thermalized carrier diffusion, and linear/nonlinear rate
235 constants affecting scintillator proportionality,” vol. 8852, pp. 88520J–
236 88520J–22, 2013.

- 237 [3] J. Q. Grim, K. B. Ucer, A. Burger, P. Bhattacharya, E. Tupitsyn, E. Rowe,
238 V. M. Buliga, L. Trefilova, A. Gektin, G. A. Bizarri, W. W. Moses, and
239 R. T. Williams, “Nonlinear quenching of densely excited states in wide-gap
240 solids,” *Phys. Rev. B*, vol. 87, p. 125117, Mar 2013.
- 241 [4] G. Bizarri, N. J. Cherepy, W. S. Choong, G. Hull, W. W. Moses,
242 S. A. Payne, J. Singh, J. D. Valentine, A. N. Vasilev, and R. T.
243 Williams, “Progress in studying scintillator proportionality: Phenomeno-
244 logical model,” *IEEE Transactions on Nuclear Science*, vol. 56, pp. 2313–
245 2320, Aug 2009.
- 246 [5] X. Lu, Q. Li, G. A. Bizarri, K. Yang, M. R. Mayhugh, P. R. Menge, and
247 R. T. Williams, “Coupled rate and transport equations modeling propor-
248 tionality of light yield in high-energy electron tracks: CsI at 295 K and 100
249 K; CsI:Tl at 295 K,” *Phys. Rev. B*, vol. 92, p. 115207, Sep 2015.
- 250 [6] X. Lu, S. Gridin, R. T. Williams, M. R. Mayhugh, A. Gektin, A. Syntfeld-
251 Kazuch, L. Swiderski, and M. Moszynski, “Energy-dependent scintillation
252 pulse shape and proportionality of decay components for csi:tl: Modeling
253 with transport and rate equations,” *Phys. Rev. Applied*, vol. 7, p. 014007,
254 Jan 2017.
- 255 [7] L. Dinca, P. Dorenbos, J. de Haas, V. Bom, and C. V. Eijk, “Alphagamma
256 pulse shape discrimination in CsI:Tl, CsI:Na and BaF₂ scintillators,” *Nu-
257 clear Instruments and Methods in Physics Research Section A: Acceler-
258 ators, Spectrometers, Detectors and Associated Equipment*, vol. 486, no. 12,
259 pp. 141 – 145, 2002. Proceedings of the 6th International Conference on
260 Inorganic Scintillators and their Use in Scientific and Industrial Applica-
261 tions.
- 262 [8] M. Kobayashi, Y. Tamagawa, S. Tomita, A. Yamamoto, I. Ogawa,
263 and Y. Usuki, “Significantly different pulse shapes for γ - and α -rays
264 in Gd₃Al₂Ga₃O₁₂:Ce³⁺ scintillating crystals,” *Nuclear Instruments and*

- 265 *Methods in Physics Research Section A: Accelerators, Spectrometers, De-*
266 *tectors and Associated Equipment*, vol. 694, pp. 91 – 94, 2012.
- 267 [9] L. Bardelli, M. Bini, P. Bizzeti, F. Danevich, T. Fazzini, N. Krutyak,
268 V. Kobychhev, P. Maurenzig, V. Mokina, S. Nagorny, M. Pashkovskii,
269 D. Poda, V. Tretyak, and S. Yurchenko, “Pulse-shape discrimination with
270 PbWO_4 crystal scintillators,” *Nuclear Instruments and Methods in Physics*
271 *Research Section A: Accelerators, Spectrometers, Detectors and Associated*
272 *Equipment*, vol. 584, no. 1, pp. 129 – 134, 2008.
- 273 [10] K. Yang, P. R. Menge, and V. Ouspenski, “Enhanced α - γ discrimination
274 in co-doped $\text{LaBr}_3\text{:Ce}$,” *IEEE Transactions on Nuclear Science*, vol. 63,
275 pp. 416–421, Feb 2016.
- 276 [11] S. Rawat, M. Tyagi, P. Netrakanti, V. Kashyap, A. Singh, D. Desai, A. Mi-
277 tra, G. A. Kumar, and S. Gadkari, “Pulse shape discrimination properties of
278 $\text{Gd}_3\text{Ga}_3\text{Al}_2\text{O}_{12}\text{:Ce,B}$ single crystal in comparison with CsI:Tl ,” *Nuclear In-*
279 *struments and Methods in Physics Research Section A: Accelerators, Spec-*
280 *trometers, Detectors and Associated Equipment*, pp. –, 2016.
- 281 [12] K. Mesick, D. Coupland, and L. Stonehill, “Pulse-shape discrimination and
282 energy quenching of alpha particles in $\text{Cs}_2\text{LiLaBr}_6\text{:Ce}^{3+}$,” *Nuclear Instru-*
283 *ments and Methods in Physics Research Section A: Accelerators, Spectrom-*
284 *eters, Detectors and Associated Equipment*, vol. 841, pp. 139 – 143, 2017.
- 285 [13] N. Zaitseva, B. L. Rupert, I. Paweczak, A. Glenn, H. P. Martinez, L. Car-
286 man, M. Faust, N. Cherepy, and S. Payne, “Plastic scintillators with ef-
287 ficient neutron/gamma pulse shape discrimination,” *Nuclear Instruments*
288 *and Methods in Physics Research Section A: Accelerators, Spectrometers,*
289 *Detectors and Associated Equipment*, vol. 668, no. Supplement C, pp. 88 –
290 93, 2012.
- 291 [14] P. Belli, R. Bernabei, R. Cerulli, C. Dai, F. Danevich, A. Incicchitti,
292 V. Kobychhev, O. Ponkratenko, D. Prospero, V. Tretyak, and Y. Zdesenko,

- 293 “Performances of a CeF_3 crystal scintillator and its application to the search
294 for rare processes,” *Nuclear Instruments and Methods in Physics Research*
295 *Section A: Accelerators, Spectrometers, Detectors and Associated Equip-*
296 *ment*, vol. 498, no. 13, pp. 352 – 361, 2003.
- 297 [15] R. Ogawara and M. Ishikawa, “Feasibility study on signal separation for
298 spontaneous alpha decay in $\text{LaBr}_3\text{:Ce}$ scintillator by signal peak-to-charge
299 discrimination,” *Review of Scientific Instruments*, vol. 86, no. 8, 2015.
- 300 [16] C. M. Whitney, L. Soundara-Pandian, E. B. Johnson, S. Vogel, B. Vinci,
301 M. Squillante, J. Glodo, and J. F. Christian, “Gammaneutron imaging
302 system utilizing pulse shape discrimination with clyc,” *Nuclear Instruments*
303 *and Methods in Physics Research Section A: Accelerators, Spectrometers,*
304 *Detectors and Associated Equipment*, vol. 784, no. Supplement C, pp. 346 –
305 351, 2015. Symposium on Radiation Measurements and Applications 2014
306 (SORMA XV).
- 307 [17] R. Cerulli, P. Belli, R. Bernabei, F. Cappella, F. Nozzoli, F. Montecchia,
308 A. d’Angelo, A. Incicchitti, D. Prospero, and C. Dai, “Performances of a
309 BaF_2 detector and its application to the search for decay modes in ^{130}Ba ,”
310 *Nuclear Instruments and Methods in Physics Research Section A: Acceler-*
311 *ators, Spectrometers, Detectors and Associated Equipment*, vol. 525, no. 3,
312 pp. 535 – 543, 2004.
- 313 [18] A. Syntfeld-Kazuch, M. Moszyński, L. Świdorski, W. Klamra, and A. Nas-
314 salski, “Light pulse shape dependence on γ -ray energy in $\text{CsI}(\text{Tl})$,” *IEEE*
315 *Transactions on Nuclear Science*, vol. 55, pp. 1246–1250, June 2008.
- 316 [19] W.-S. Choong, G. Bizarri, N. Cherepy, G. Hull, W. Moses, and S. Payne,
317 “Measuring the dependence of the decay curve on the electron energy de-
318 posit in $\text{NaI}(\text{Tl})$,” *Nuclear Instruments and Methods in Physics Research*
319 *Section A: Accelerators, Spectrometers, Detectors and Associated Equip-*
320 *ment*, vol. 646, no. 1, pp. 95 – 99, 2011.

- 321 [20] X. Wen and A. Enqvist, “Measuring the scintillation decay time for dif-
322 ferent energy deposited by γ -rays and neutrons in a $\text{Cs}_2\text{LiYCl}_6:\text{Ce}^{3+}$ de-
323 tector,” *Nuclear Instruments and Methods in Physics Research Section A: Accelerators, Spectrometers, Detectors and Associated Equipment*, vol. 853,
324 no. Supplement C, pp. 9 – 15, 2017.
- 326 [21] L. Świdorski, n. Marek Moszy A. Syntfeld-Kazuch, M. Szawłowski, and
327 T. Szcześniak, “Measuring the scintillation decay time for different energy
328 depositions in NaI:Tl, LSO:Ce and CeBr_3 scintillators,” *Nuclear Instru-*
329 *ments and Methods in Physics Research Section A: Accelerators, Spectrom-*
330 *eters, Detectors and Associated Equipment*, vol. 749, no. Supplement C,
331 pp. 68 – 73, 2014.
- 332 [22] S. W. Smith, *The Scientist and Engineer’s Guide to Digital Signal Process-*
333 *ing*. San Diego, CA, USA: California Technical Publishing, 1997.